Nonlinear Studies
Vol. 11, No. 3, pp. 319-344, 2004

Nonlinear Studies

Daytona Beach, FL 2004

The dialogue between data and model: Passive stability and relaxation behavior in a ball bouncing task

Tjeerd M. H. Dijkstra[1], Hiromu Katsumata[2,3], Aymar de Rugy[2] and Dagmar Sternad[2]

[1]Department of Psychology, The Ohio State University
1885 Neil Avenue, Columbus, OH 43210, USA.
E-mail: t.dijkstra@science.ru.nl

[2]Department of Kinesiology, Pennsylvania State University
266 Rec Hall, University Park PA 16802, USA.
E-mail: dxs48@psu.edu

[3]Department of Sports and Health Science, Juntendo University
Chiba, Japan.
E-mail: hiromu@xd6.so-net.ne.jp

Abstract We investigate the skill of rhythmically bouncing a ball on a racket with a focus on the mathematical modeling of the stability of performance. As a first step we derive the deterministic ball bouncing map as a Poincaré section of a sinusoidally driven bouncing ball. Subsequently, we show the ball bouncing map to have a passively stable regime. More precisely, for negative racket acceleration at impact, no control of racket amplitude or frequency is necessary for stable performance. Support for the model comes from a motor learning study, where a decrease in variability covaries with a change of mean acceleration at impact towards more negative values. For a more fine-grained test of the model we develop a stochastic version of it, by adding Gaussian white noise to the dynamics. We then test the model predictions for the correlation functions. We find that the observed correlation functions match the theoretical ones quite well, lending new support for the model. Lastly, we compare the observed recovery from a sudden change with which the ball leaves the racket with model predictions. We find a mismatch between data and model in the sense that the model is too "slow". We take this failure of the ball bouncing model as an impetus to further develop the model. In the perturbation study, we observe a significant modulation of the racket period but not of the racket amplitude. Thus, racket period seems a candidate state variable that should be included the ball bouncing map.

[0]2000 *Mathematics Subject Classification: Primary* 37H20; Secondary: 93C55
Keywords: dynamical systems, motor control, rhythmic movements.

1 Introduction

Human motor behavior constitutes physical actions that are embedded in and coupled to the physical environment. The body creates and is subject to forces that provide constraints for the execution of actions. This behavioral level of analysis has been one important point of entry for theorizing about the control of human movements. While the neurophysiological substrate provides the structural and functional underpinnings for biological systems, tasks and task performance are typically defined at the behavioral level of analysis. For instance, hitting a ball with a racket to strike a target requires that the ball is hit and released with a certain velocity such that its flight trajectory travels the desired distance to the target. Adopting this level of analysis, task performance can be understood as a complex system which is defined over the executing limbs or chains of effectors and the objects of the environment. Coupling between these system components is provided by mechanical and informational links, such as contact dynamics, gravity, ballistic flight, and visual or haptic information.

In a series of studies Sternad and colleagues investigated the simple mechanical task of bouncing a ball rhythmically on a racket as an exemplary perceptual-motor skill in which dynamical stability plays a central role [15, 13, 14, 9]. The actor (or actuator) holds a racket in his/her hand and hits a ball into the air keeping a consistent period and amplitude. Sensory information is required to adjust the racket's position and velocity when hitting the ball to achieve the desired target height. Feedback information may be used to correct for errors in performance. This "toy task" of bouncing a ball has received considerable attention in both the robotics and the motor control literature as it poses many fundamental control and sensory problems [1, 2].

In the applied mathematics literature the cyclic ball-racket interactions have been modeled by a nonlinear discrete dynamical system, the *ball bouncing map*, which we will rederive in the next section. There, it provided a study case to investigate dynamical stability of different attractor states and the period-doubling route to chaos, see [19] and the references therein. A typical experimental set-up to study this system consists of a small ball bearing and a periodically driven loud speaker. The model consists of a periodically moving table (speaker) impacting a particle (ball bearing) which follows ballistic flight. Different attractor states were indeed observed when the frequency of the speaker was manipulated.

The application of this model to human performance was first advanced by Sternad, Schaal, and colleagues in a series of studies using an experimental set-up that closely mimicked the physical model [15]. They showed that the ball bouncing map had a stable period-1 attractor when the table impacts the ball with a negative acceleration. The significance of this theoretical finding for human performance is that humans can perform the task by choosing the right acceleration without using any error-correction. This coordination strategy has the advantage that perturbations of the system relax back to the stable attractor, provided they are sufficiently small. This inherent compensatory behavior obviates the need for active error corrections by the actor to return to and maintain stable performance. Sternad and Schaal termed this type of stability that can be achieved without any control *passive stability*. Rephrased in terms of control theory, the system has

a parameter regime where the open-loop control is sufficient to provide stability. In this conceptualization, active stability includes feedback information. This distinction between active and passive stability was made by McGeer [10] in the work on passive dynamic walking.

The experimental question addressed in the previous studies was whether humans make use of this passive stability by hitting the ball with a negative racket acceleration. The task by no means prescribes such a strategy, since a stable pattern can also be achieved with impacts with positive acceleration when supplemented by feedback information from the ball trajectory, as the robot juggler of Koditschek and Bühler [1, 2] has shown. The hypothesis was that humans perceive and attune to the fixed point attractor that specifies the period-1 solution and thereby exploit the dynamical stability of this task. Experimental data confirmed these quantitative predictions in a number of different experiments. Some of these results will be briefly reviewed below, as they motivated the present study and provide a departure point for developing and testing more finer-grained predictions of the model. These predictions will be tested against results obtained from a virtual ball bouncing set-up where subjects hold a physical racket (that they cannot see) and see and manipulate a virtual racket and ball on a large screen.

As a first step in the present study we derive the two-dimensional discrete dynamical system describing the ball and racket motion, the so-called *ball bouncing map*. While this model is almost identical to the one in the previous studies, it will be derived again for three reasons: (1) The derivation introduces a different definition of the state variables in preparation for the model extension. (2) The derivation uses a seemingly more restricted assumption of the racket motion as a sine wave, whereas in the older studies the racket motion was only assumed to be periodic. However, this restriction will allow to make more quantitative predictions about the stationary state and the relaxation behavior. (3) Overall, the derivation is considerably more detailed and thereby presents several new facts that allow new predictions and conclusions about human performance.

This paper is structured as follows: in section 2, the state space with its three state variables (ball position and velocity and racket position) will be introduced and the two-dimensional discrete map, the *ball bouncing map*, is derived by performing a Poincaré section. In section 3, the fixed points of the map are calculated and their domains of attraction are numerically investigated. In section 4, a linear stability analysis of the fixed points is performed and predictions are formulated. In section 5, experimental evidence is reviewed in support of a first set of coarse-grained predictions from the ball bouncing map. In section 6 we compare the fluctuations around the stationary state from a steady performance with the theoretical predictions. The comparison is made between the correlation functions from the experiment and the theoretical ones. In section 7 we compare the impulse response of the model to a perturbation of velocity just after impact with a data set collected for this purpose. In section 8 we summarize and discuss our findings.

2 The ball bouncing map

The state of the ball is specified by its position $x_b(t)$ and velocity $v_b(t)$ (see Figure 1). Both racket and ball motion are confined to the vertical dimension in order

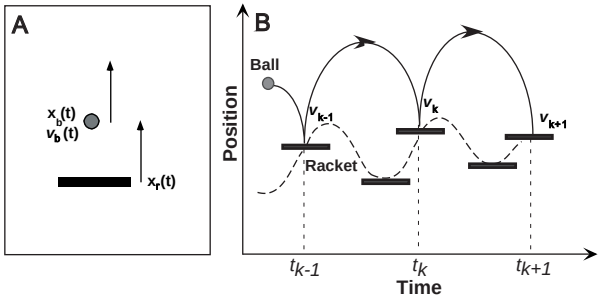

Figure 1: Overview of the task and the state space variables. The left panel (A) indicates the continuous state space variables, ball position $x_b(t)$, ball velocity $v_b(t)$ and racket position $x_r(t)$. The right panel (B) illustrates a schematized performance with three bounces indicated at time t indexed by their iteration k. The panel also summarizes the discrete state space variables: time of occurrence of a bounce t_k and ball velocity directly after a bounce v_k.

to keep the model tractable. If we denote the time of last (k-th) impact with t_k, the ball trajectory between two bounces follows ballistic flight and the equations can be written as:

$$x_b(t) = x_b(t_k) + v_b^+(t - t_k) - \frac{g}{2}(t - t_k)^2, \quad (1)$$

$$v_b(t) = v_b^+ - g(t - t_k), \quad (2)$$

with $t_k < t < t_{k+1}$. v_b^+ denotes the ball velocity just after the k-th impact and g stands for the acceleration due to gravity. In this derivation we assumed the friction of the air to be negligible. To go from one bounce to the next, we need to consider what happens when the ball impacts the racket. We assume an instantaneous inelastic impact as follows:

$$\alpha(v_b^-(t_k) - v_r^-(t_k)) = -(v_b^+(t_k) - v_r^+(t_k)), \quad (3)$$

with parameter α as the coefficient of restitution. The superscript $^-$ denotes velocities before impact, the superscript $^+$ denotes velocities after impact, and v_r is the velocity of the racket. Thus, the difference in velocity between racket and ball after impact is a fraction α of the difference before impact. The approximation of the impact as being instantaneous is an idealization of the impact observed in real performance. In a study of the impact dynamics in ball bouncing with different values of α, ranging between 0.5 and 0, [9] showed that the duration of the contact is on average 30 ms and extends up to 116 ms for completely nonelastic ball contacts, i.e., $\alpha = 0$. However, in most previous experiments α was equal or higher than 0.5. Thus, the duration of the contact is relatively short and does not affect the control of the racket movement. Another assumption is that α is a constant. For a real racket, the coefficient of restitution depends on where the ball hits the racket, being larger at the edges of the racket surface than in the middle. These assumptions were largely satisfied by constraining the ball-racket

contact position in the physical experimental set-ups. For the experiments run in the virtual environment, the assumptions of instantaneous contact and constancy of the coefficient of restitution become exact.

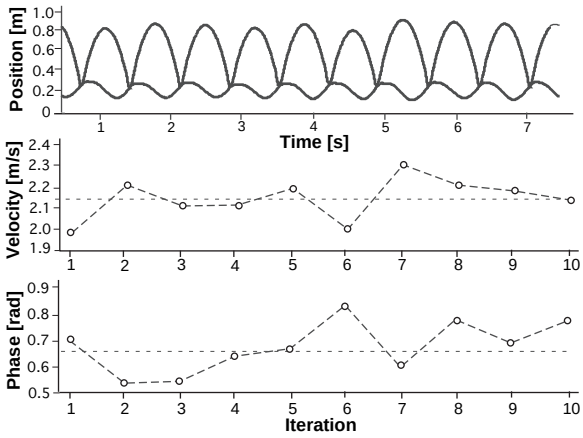

Figure 2: Exemplary data. The top panel shows the continuous trajectories of ball and racket. The middle and bottom panels show the discrete state variables across the same 10 bounces/iterations: ball velocity after impact v_k and phase of impact θ_k. These variables are extracted from the continuous data as plotted in the top panel. The dashed horizontal lines denote the sample mean values.

The state of the racket is described by its position ($x_r(t)$) (see Figure 1). The movement is assumed to be a sine-wave with fixed amplitude a_r and constant frequency ω_r in units of rad/s. Formally:

$$x_r(t) = a_r \sin(\omega_r t), \tag{4}$$

An exemplary performance in Figure 2 illustrates that the sine-wave assumption is reasonable. The assumption also remains tenable if one considers that the ball impact perturbs the racket trajectory. Since these perturbations occur immediately after the impact and and die out after approximately 100 ms, far from the next impact, they can be safely ignored. The sine-wave assumption is a change from previous derivations of the ball bouncing map in the human motor control context. In [15] and subsequent papers the only assumption made about the racket trajectory was that it is periodic. That assumption turned out to be sufficient to draw conclusions about stability (see section 4). While it is certainly elegant to derive conclusions from minimal assumptions, it is clear that a sine wave is a good first-order approximation for the racket trajectory. The additional advantage of the assumption of a sine-wave with fixed parameters is that it permits the derivation of predictions about the stationary state and its domain of attraction. As a final point, note that the velocity of the racket ($v_r(t)$) is not an independent degree of freedom (and thus not a dimension of state space) since $v_r(t)$ can be derived from the racket position by differentiation with respect to time. Explicitly,

$$v_r(t) = a_r \omega_r \cos(\omega_r t).$$

We further assume that the racket is much heavier than the ball and thus the racket velocities before and after the impact are identical, i.e. $v_r^-(t_k) = v_r^+(t_k) = a_r\omega_r \cos(\omega_r t_k)$

The equations 1, 2, and 4, combined with the boundary condition 3 constitute a two-dimensional non-autonomous continuous dynamical system, i.e. a system explicitly dependent on time, which is equivalent to a three-dimensional autonomous dynamical system [18]. We proceed by taking the Poincaré section at the time of impact, resulting in a two-dimensional discrete dynamical system with the discrete state variables time of impact (t_k) and velocity of the ball after impact (v_k), see Figure 1 right panel. Note that the subscripts r and b are no longer necessary as there is only one velocity. The system has four parameters: coefficient of restitution (α), acceleration of gravity (g), and amplitude (a_r) and frequency (ω_r) of the racket motion. By substituting the racket position eq. 4 (at times $t = t_k$ and $t = t_{k+1}$) for the ball position in eq. 1 at $t = t_{k+1}$, we obtain the first equation of the ball bouncing map, the *time map*:

$$0 = a_r(\sin(\omega_r t_k) - \sin(\omega_r t_{k+1})) + v_k(t_{k+1} - t_k) - \frac{g}{2}(t_{k+1} - t_k)^2.$$

This is an implicit equation for the time of occurrence of the next impact t_{k+1} given the current state of the system (t_k, v_k). The fact that the map is implicit poses no impediment to the theoretical analysis, since one can use the implicit function theorem to find the derivatives of the map. In the simulations we solve the system by using a numerical zero finder.

From the equation for ball velocity at $t = t_{k+1}$ (eq. 2) and the impact equation (eq. 3), we obtain the second equation of the ball bouncing map, the *velocity map*:

$$v_{k+1} = (1 + \alpha)a_r\omega_r \cos(\omega_r t_{k+1}) - \alpha v_k + g\alpha(t_{k+1} - t_k).$$

This is an explicit equation for the velocity of the ball directly after the impact. The functional form of the time and velocity maps differs from the equations presented in previous work [15, 14] since the state variable had been defined as the velocity before impact. While the velocity before impact is easier to extract from the experimental data, the choice of velocity after impact is mathematically more convenient. Further, we proceed to use the phase of impact in the racket cycle as a state variable instead of the time of impact, again for reasons of mathematical convenience. Defining the phase of impact by:

$$\theta_k = \omega_r t_k,$$

we arrive at the final *ball bouncing map*:

$$v_{k+1} = (1 + \alpha)a_r\omega_r \cos(\theta_{k+1}) - \alpha v_k + \frac{g\alpha}{\omega_r}(\theta_{k+1} - \theta_k), \quad (5)$$

$$0 = a_r\omega_r^2(\sin(\theta_k) - \sin(\theta_{k+1})) + v_k\omega_r(\theta_{k+1} - \theta_k) - \frac{g}{2}(\theta_{k+1} - \theta_k)^2, \quad (6)$$

where the implicit phase equation has been multiplied with ω_r^2 for simplification. An exemplary series of these two discrete state variables extracted from the continuous time series of human performance is shown in Figure 2 in the middle and bottom panel.

3 The period-1 attractor of the ball bouncing map

In this and the following section we perform a linear stability analysis of the ball bouncing map [16]. As the first step, we determine the fixed points, denoted by $(\tilde{v}, \tilde{\theta})$, by setting:

$$\begin{aligned} v_{k+1} = v_k &= \tilde{v}, \\ \theta_{k+1} = \theta_k + 2\pi &= \tilde{\theta}. \end{aligned}$$

Substitution of the variables at k and $k+1$ in the ball bouncing map (eqs. 5, 6) leads to:

$$\tilde{v} = \frac{\pi g}{\omega_r}, \tag{7}$$

$$\cos(\tilde{\theta}) = \pi \frac{1-\alpha}{1+\alpha} \frac{g}{\omega_r^2 a_r}. \tag{8}$$

This solution defines the fixed point (stationary state) of the ball bouncing map. Three remarks about this stationary state are in place. First, since the map is derived by taking the Poincaré section of a continuous dynamical system, the fixed point of the map is a period-1 or limit cycle attractor of the continuous dynamics. From now onwards, we will use the term "fixed point", "stationary state" and "period-1 attractor" interchangeably. Second, the "stationary" state is not strictly stationary since phase θ_k increases by 2π between each bounce. We could have used the wrapped phase as state variable, denoted by $\theta_k \bmod 2\pi$, which has a true stationary state. However, in the analysis we will use the unwrapped phase as it is easier to solve the implicit phase equation if the zero finder only has to search for solutions in one direction, since the next phase has to be larger than the current one. However, in all plots we will display wrapped phase. Third, since $g > 0$ and $\omega_r > 0$, the velocity after impact at the stationary state is necessarily positive, i.e., $\tilde{v} > 0$. Given the next predictions about negative ball acceleration that follow below, it should be kept in mind that this condition of positive ball velocity always has to be satisfied.

The ball bouncing map possesses other attractors besides the period-1 attractor. In particular, we note the existence of "sticking solutions" [19, p 38], which coexist with the period-1 attractor of eqs. 7 and 8. Figure 3 presents an example of both attractors. The top panel shows the period-1 attractor, which looks similar to the behavior displayed by human subjects as illustrated in Figure 2. The bottom panel shows the sticking solution where the ball sticks to the racket for at least a part of the racket trajectory. For both attractors, equations 1, 2, 3 and 4 were iterated with a fourth-order Runge-Kutta algorithm with time step of 1 ms. We used the following parameter values: $\alpha = 0.5$, $g = 9.81$ m/s^2, $\omega_r = 2\pi/0.92$ rad/s, $a_r = 0.30$ m. For both panels the initial position of the ball was $x_b(0) = 0.205$ m. The only difference between the two simulations were the initial values of velocity. In the top panel the initial value of the ball velocity was $v_b(0) = 4.8$ m/s whereas in the lower panel it was $v_b(0) = 5.7$ m/s. This coexistence of solutions means that, depending on the initial condition, the system can end up either in the period-1 attractor or in a sticking solution. For the understanding of human behavior, this points to an interesting conclusion: since sticking solutions

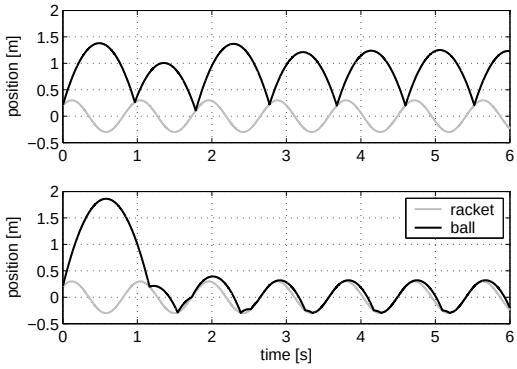

Figure 3: A period-1 attractor (top panel) and a sticking solution (bottom panel) coexist for the same parameter values. However, the initial conditions were different (see text).

have only rarely been observed in experiments, it can be inferred that subjects are able to avoid such sticking solutions. At the same time, though, subjects are able to parameterize the ball bouncing system to establish the stable regime (as will be reviewed below). This means that they are sensitive to how they initialize the performance. For example, when starting periodic bouncing with the ball resting on the racket, the actor not only creates a parameterization of the racket that affords stability, but also establishes the correct initial conditions to avoid sticking solutions.

Given the dependency on initial conditions, one would like to know for which initial values (v_0, θ_0) the system ends up at the period-1 attractor. This region of initial conditions is called the *domain of attraction* of the period-1 attractor. Since there is no analytical route to calculate the domain of attraction, numerical simulations have to be performed. Figure 4 shows the domain of attraction of the period-1 attractor as a function of the initial phase θ_0 and and velocity v_0. When the initial conditions are in the white region, the system ends up at the period-1 attractor which is denoted by a black dot. In particular, for the initial condition of the black cross just above the dot, the system ends up at the period-1 attractor. This particular condition is plotted in the top panel of Figure 3. When the initial conditions are in the gray region, the system ends up at a sticking solution. In particular, for the initial conditions of the top black cross, the system ends up in the sticking solutions illustrated in Figure 3 bottom panel. The black region denotes the area below the racket which is inaccessible for initial values above the racket. Above the black region we find a region of sticking initial conditions: here the initial velocity is too low and the ball ends up sticking to the racket. Above that region we find a band of period-1 initial conditions: the ball ends up at the period-1 attractor within a few dozen bounces. For higher initial velocities the domain of attraction has a complicated structure.

The details of the simulation were as follows. The simulation was implemented in Matlab 6.5. As zero finder we used Matlab's built-in "fzero", which is based

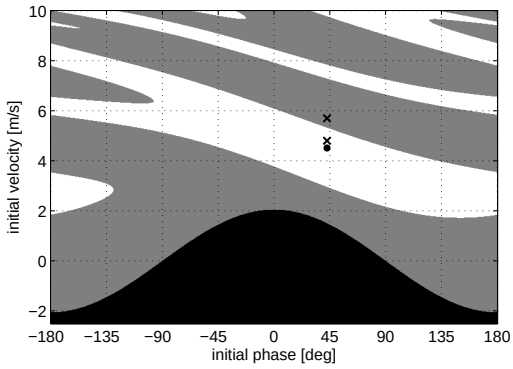

Figure 4: Domain of attraction of period-1 attractor. For an initial condition in the white region the system ends up at the period-1 attractor, for the gray region it ends up at a sticking solution. The black region is inaccessible since it is below the racket. The black dot denotes the period-1 attractor $\tilde{v}, \tilde{\theta}$ as defined in eqs. 7 and 8 and the two crosses denote the initial conditions used in Figure 3.

on the van Wijngaarden-Dekker-Brent method [12], with a tolerance set to 10^{-12}. We iterated the ball bouncing map (eqs. 5 and 6) for 100 iterations, stopping the iteration when one of three conditions occurred: (1) both the velocity and the phase were within 10^{-3} of the period-1 attractor. In this case we colored the starting condition white in Figure 4. (2) The time between bounces was less than 10^{-3} s. In this case we colored the starting condition grey in Figure 4. (3) The velocity with which the ball leaves the racket is lower than the racket velocity. In this case we colored the starting condition black in Figure 4. The simulation never ran to the maximum of 100 iterations, showing that the system had relaxed to one of the attractors within the tolerances used. The results depend very weakly on the various tolerances used. We used the same values for the parameters as for the simulations plotted in Figure 3. Explicitly: $\alpha = 0.5$, $g = 9.81$ m/s^2, $\omega_r = 2\ \pi/0.92$ rad/s, $a_r = 0.30$ m.

4 Linear stability of the ball bouncing map

In order to analyze the linear stability of the period-1 attractor (eqs. 7 and 8) the Jacobian has to be derived. To this end the partial differentials of the two state variables v_{k+1}, θ_{k+1} have to be calculated. Since the phase map eq. 6 is implicit, the implicit function theorem can be used to calculate the partial derivatives of phase with respect to the two state variables [7]. Denoting the right-hand side of the phase map by $F(\theta_{k+1}, \theta_k, v_k)$, the differential dF is:

$$dF = \left(-a_r \cos(\theta_{k+1}) + \frac{v_k}{\omega_r} - \frac{g}{\omega_r^2}(\theta_{k+1} - \theta_k)\right) d\theta_{k+1} + \left(a_r \cos(\theta_k) - \frac{v_k}{\omega_r} + \frac{g}{\omega_r^2}(\theta_{k+1} - \theta_k)\right) d\theta_k + \frac{1}{\omega_r}(\theta_{k+1} - \theta_k) dv_k.$$

The partial derivatives of θ_{k+1} evaluated at the fixed point $(\tilde{v}, \tilde{\theta})$ are:

$$\left.\frac{\partial \theta_{k+1}}{\partial \theta_k}\right|_{(\tilde{v},\tilde{\theta})} = \left. -\frac{\frac{\partial F}{\partial \theta_k}}{\frac{\partial F}{\partial \theta_{k+1}}}\right|_{(\tilde{v},\tilde{\theta})} = 1,$$

$$\left.\frac{\partial \theta_{k+1}}{\partial v_k}\right|_{(\tilde{v},\tilde{\theta})} = \left. -\frac{\frac{\partial F}{\partial v_k}}{\frac{\partial F}{\partial \theta_{k+1}}}\right|_{(\tilde{v},\tilde{\theta})} = (1+\alpha)\omega_r/g.$$

Calculation of the partial derivatives of v_{k+1} is straightforward since the velocity map (eq. 5) is explicit. Using these results, the Jacobian of the ball bouncing map can be determined and evaluated at the fixed point $(\tilde{v}, \tilde{\theta})$:

$$J(\tilde{v},\tilde{\theta}) \equiv \begin{pmatrix} \frac{\partial v_{k+1}}{\partial v_k} & \frac{\partial v_{k+1}}{\partial \theta_k} \\ \frac{\partial \theta_{k+1}}{\partial v_k} & \frac{\partial \theta_{k+1}}{\partial \theta_k} \end{pmatrix} = \begin{pmatrix} \alpha^2 - (1+\alpha)^2 a_r \omega_r^2 \sin(\tilde{\theta})/g & -(1+\alpha) a_r \omega_r \sin(\tilde{\theta}) \\ (1+\alpha)\omega_r/g & 1 \end{pmatrix}, \tag{9}$$

where $\sin(\tilde{\theta})$ depends on α, ω_r, a_r and g through eq. 8. The Jacobian can be simplified by noting that $-a_r\omega_r^2 \sin(\tilde{\theta})$ equals the racket acceleration at impact. Denoting the racket acceleration at impact in units of g by $AC \equiv -a_r\omega_r^2 \sin(\tilde{\theta})/g$, the eigenvalues of the Jacobian are given by the solutions $\lambda_\pm$ of the characteristic equation:

$$\lambda^2 - ((1+\alpha^2) + (1+\alpha)^2 AC)\lambda + \alpha^2 = 0.$$

We note that linear stability is determined by the pair (α, AC), where AC depends on the four parameters of the ball bouncing map. Substituting for $\sin(\tilde{\theta})$, the racket acceleration at impact AC is written in explicit form:

$$AC = -\sqrt{\left(\frac{a_r\omega_r^2}{g}\right)^2 - \pi^2 \left(\frac{1-\alpha}{1+\alpha}\right)^2}.$$

Continuing the calculation of the eigenvalues, one more definition is introduced for simplification $c \equiv ((1+\alpha^2) + (1+\alpha)^2 AC)/2$. Hence, the two eigenvalues are expressed as:

$$\lambda_\pm = c \pm \sqrt{c^2 - \alpha^2}. \tag{10}$$

The condition for stability of the period-1 attractor is that the absolute value of both eigenvalues must be smaller than 1 (see [16, p 126]). We first consider the case of the eigenvalues forming a complex pair, i.e., $c^2 < \alpha^2$. The boundaries of the regime where the eigenvalues are complex can be obtained from the condition $c^2 = \alpha^2$ and lead to:

$$-\left(\frac{1-\alpha}{1+\alpha}\right)^2 < AC < -1. \tag{11}$$

Figure 5 shows the *ball bouncing stability diagram*, i.e., the region in parameter space where the ball bouncing map has a linearly stable period-1 attractor. As the eigenvalues only depend on α and AC, the conditions for stability can be visualized as a region in a two-dimensional plot. The boundaries defined by the complex eigenvalues are indicated by grey lines. Since the eigenvalues form a

complex pair, their absolute values are identical, i.e., $|\lambda_+| = |\lambda_-|$. Furthermore, since $\lambda_+\lambda_- = (c + \sqrt{c^2 - \alpha^2})(c - \sqrt{c^2 - \alpha^2}) = c^2 - (c^2 - \alpha^2) = \alpha^2$, we have:

$$|\lambda_+| = |\lambda_-| = |\alpha|. \tag{12}$$

Thus, when the eigenvalues are complex, their absolute value equals the coefficient of restitution. From the condition that the absolute values of the eigenvalues have to be smaller than 1, we obtain two stability boundaries as follows:

$$|\alpha| < 1. \tag{13}$$

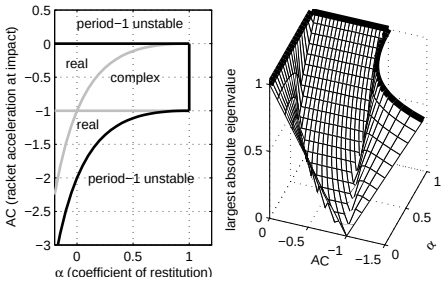

Figure 5: Left panel: Stability diagram of the ball-bouncing map (eqs. 5, 6). The boundaries of stability indicated in black are given by eq. 14 and eq. 13. Also indicated are the boundaries between the real and complex regions, as given by eq. 11 and indicated by grey curves. The eigenvalues are also complex in the region between the grey curves between $-0.2 < \alpha < 0$, which was too small to label. Right panel: eigenvalue with the largest absolute value, plotted as a function of AC and α. The eigenvalue is only plotted as long as its absolute value is smaller than 1, i.e., within the stability boundaries.

We now consider the case when the eigenvalues are real, i.e., $c^2 > \alpha^2$. Straightforward but tedious algebra yields the following stability boundaries:

$$-2\left(\frac{1+\alpha^2}{(1+\alpha)^2}\right) < AC < 0. \tag{14}$$

In Figure 5 left panel, the curves of the stability boundaries defined by real eigenvalues are plotted as black curves. These boundaries encompass the ones found before for complex eigenvalues (eq. 11). Thus, the boundaries of stability are given by eq. 14 and eq. 13. The right panel of Figure 5 affords another view of the stability diagram. Here, the eigenvalue with the largest absolute value is plotted, i.e., the one that determines stability, as a function of AC and α. The eigenvalue is only plotted where it is smaller than 1 in absolute value. Only the stable regime of the ball bouncing map is plotted, such that the top rim corresponds to the boundary of the stable regime. For a fixed α the figure shows a flat region flanked by slopes of increasing absolute eigenvalue, indicating less stability. We also observe that the flat surface rises with increasing α. This flat surface corresponds to

the region labeled "complex" in the left panel Figure 5 and we know from eq. 12 that the absolute values of both eigenvalues equal the value of the coefficient of restitution α.

The comparison of the behavior of human subjects and the fine-grained model predictions in section 7 will reveal that the absolute values of the eigenvalues of the model are too large. This raises the question for which parameter values the eigenvalues are the smallest. Since the experiments are performed at a fixed coefficient of restitution α, we answer the question for which values of AC are the absolute values of the eigenvalues minimal. We aim to show that, for a given α, the minimum absolute value of the larger of the two eigenvalues is larger than, or equal to α. Formally:

$$\min_{AC \in S} \max(|\lambda_+|, |\lambda_-|) \geq \alpha,$$

with S denoting the stable regime in Figure 5 left panel. These minimal absolute eigenvalues are realized in part of Figure 5 where the eigenvalues are complex, or alternatively where eq. 11 holds. In the right panel of Figure 5 these eigenvalues are realized on the flat inclined planar section. We now proceed with a formal proof.

In the region in Figure 5A labeled "complex" both eigenvalues are equal to α in absolute value (eq. 12). Hence, only the sections labeled "real" need to be considered. The top section labeled "real" of Figure 5 has boundaries $0 < AC < -\left(\frac{1-\alpha}{1+\alpha}\right)^2$. It follows that:

$$c = ((1+\alpha^2) + (1+\alpha)^2 AC)/2 \geq 0,$$

with c as the parameter introduced above in eq. 10. Thus:

$$|\lambda_+|^2 = 2c^2 + \alpha^2 + 2c\sqrt{c^2-\alpha^2} \geq 2c^2 - \alpha^2 + 2c\sqrt{c^2-\alpha^2} = |\lambda_-|^2.$$

Thus, the + eigenvalue (λ_+) has the largest absolute value in this region. We now show that the absolute value of λ_+, considered as a function of AC, increases monotonically with AC in the top section labeled "real" of Figure 5. Thus, we want to show that:

$$\frac{d|\lambda_+(AC)|^2}{dAC} \geq 0.$$

Substitution of λ_+ from eq. 10 leads to:

$$\frac{d|\lambda_+(AC)|^2}{dAC} = (1+\alpha)^2 \left(2c + \sqrt{c^2-\alpha^2} + \frac{c^2}{\sqrt{c^2-\alpha^2}}\right) \geq 0,$$

since $c > 0$. Thus, λ_+ increases monotonically in the region $-\left(\frac{1-\alpha}{1+\alpha}\right)^2 < AC < 0$. Since $|\lambda_+| = \alpha$ at the lower boundary $AC = -\left(\frac{1-\alpha}{1+\alpha}\right)^2$ it follows that $|\lambda_+| >= \alpha$ in the top section labeled "real" of Figure 5. We can perform a similar argument for the lower section labeled "real" of Figure 5. In summary, the dominant (largest) eigenvalue of the ball bouncing map for a given coefficient of restitution α has the value α.

The formal derivation that the ball bouncing map is fastest in the region labeled "complex" in the left panel of Figure 5 is illustrated in Figure 5, right panel. The region labeled "complex" in the left panel corresponds to the flat region in the middle of the range of AC values. This flat region rises with increasing α. Indeed we know from the derivation above that the height equals α.

5 Coarse-grained predictions from the ball bouncing map and their experimental support

From the analysis of the ball bouncing map above several predictions can be extracted for human performance. The first set of predictions is called "coarse-grained" and does not depend on the numerical values of the eigenvalues. The first coarse-grained model prediction is that the stable regime of the ball bouncing map affords a stable solution for subjects performing rhythmic ball bouncing. For example, for $\alpha = 0.5$, AC should be between 0 and -1.11 g. If subjects chose to perform within the stable regime, small perturbations of the ball trajectory need not be compensated for by the racket.

Stability of performance was tested in a series of previous experiments [15, 13, 14, 9]. The first support was presented in a study by Schaal et al. [15]. In a constrained task, experienced subjects moved a handle that was linked through a pantograph to a paddle which confined its motion to the vertical dimension and ensured that the surface of the racket remained strictly horizontal, in close analogy to the model. The ball was suspended on a boom and thereby also constrained to a one-dimensional flight trajectory. Subjects were instructed to contact the ball rhythmically to achieve a constant self-chosen target height. The primary dependent measure was the acceleration of the racket just before the impact AC, reflecting how subjects controlled the racket's movement for the ball contact. Averages and standard deviations were calculated over all ball-racket contacts of one trial which consisted of approximately 40 consecutive bounces. Several trials were performed for each of three target amplitude conditions and two gravity conditions. Results showed that the means of racket acceleration were negative and within the predicted range of [-0.5 g, -0.3 g] which is squarely in the stable regime as depicted in Figure 5. Importantly, some subjects showed positive AC values, indicating that negative acceleration is not a necessary solution.

In a subsequent study, relatively inexperienced subjects performed a sequence of 40 trials (40 s each) of the same condition [13]. We calculated means of racket acceleration at impact (AC) and standard deviations of ball amplitude (SDA) from each trial. Figure 6 combines the results of both dependent measures of a single subject, plotted as a function of trial number. The values of racket acceleration again support that subjects chose to hit the ball with negative racket accelerations. The variability of ball amplitude decreased significantly over practice, indicating improving performance. Further, this impact parameter showed a systematic trend towards more negative values in the same range as in the previous experiment, i.e., the range which is squarely in the stable regime. In this region, larger fluctuations are less likely to perturb the system. This trend provides support that human actors are not only sensitive to dynamical stability but

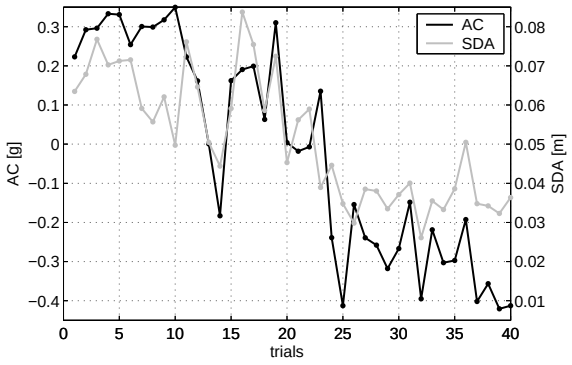

Figure 6: Results from a learning study of ball bouncing across a sequence of 40 trials, shown for a single subject. Black curve: Trial means of racket acceleration at impact in units of g. Grey curve: Standard deviation of ball amplitude.

also optimize their performance to exploit the advantages that this regime offers.

It is worth pointing out that the most energy efficient way of performing the task is to hit the ball with zero acceleration because at this moment the racket has the highest velocity leading to a given amplitude with least effort. Further, the strategy of exploiting the stable regime can also be contrasted with the control strategy implemented in a robotics study by Bühler and Koditschek [1]. They constructed an actuator which controlled the rhythmic racket movements that tracked the ball velocity in a continuous fashion. The velocity of the racket mirrored the one of the ball leading to ball-racket contacts with positive racket acceleration. According to the analysis above, this corresponds to an unstable regime. As a consequence, all perturbations need to be corrected for, which makes control computationally more expensive.

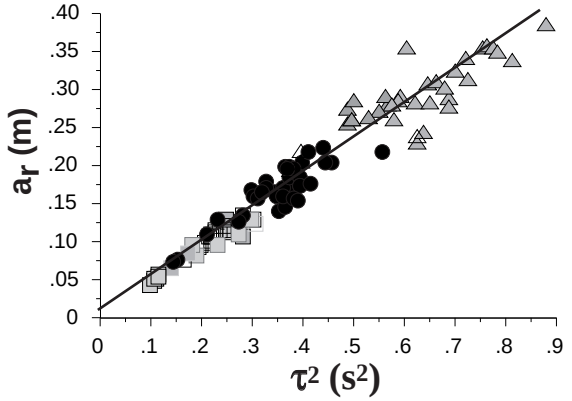

Figure 7: Trial means of racket amplitude regressed on the square of the trial mean of racket period.

The second coarse-grained model prediction derives from the dependence of the stationary state eqs. 7 and 8 on the four parameters. In their 1996 study [15], Schaal et al. reported a linear relationship between the period between bounces $\tau = 2\pi/\omega_r$ and the racket amplitude a_r, when subjects were instructed to bounce the ball to different target heights. This observed relationship between racket period and amplitude can be formally derived by rewriting eq. 8:

$$a_r = \frac{1}{4\pi}\frac{1-\alpha}{1+\alpha}\frac{g}{\cos(\tilde{\theta})}\tau^2, \tag{15}$$

Assuming $\tilde{\theta}$ to be independent of target height, this predicts a linear relationship between racket amplitude a_r and period squared τ^2.

Katsumata and Sternad (in preparation) tested this model prediction in an experiment comparing performance with and without visual information, where each visual condition was performed at three different ball target heights. For each 40 s trial, the average racket amplitude (a_r) and period (τ) were calculated. The trial estimates of a_r were regressed against the square of the trial estimates of τ. Figure 7 shows the linear regression performed for all trials of six relatively inexperienced subjects, pooled over vision and no-vision conditions. The R^2 values for the vision and no-vision condition were 0.98 and 0.90, respectively. While a scaling of the racket amplitude with the bouncing period or ball amplitude is not counterintuitive, the exact scaling of the two parameters is not trivial. Two further predictions can be derived from eq. 15: (1) the slope of the relation between a_r and τ can be computed from the data as all parameters are known and $\tilde{\theta}$ can be calculated from the data. (2) The intercept of the regression is zero. While prediction 1 has not been tested for the data, inspection of Figure 7 shows that the intercept is indeed close to zero.

In sum, these selected data of steady state performance of human actors provide support that the model captures a set of basic components of human behavior. In order to develop a finer-grained set of tests for the presence of stability in human ball bouncing, we proceed to examine the model's behavior with noise.

6 Finer-grained predictions: correlation structure in a stochastic model and data

In this and the following section, we look at predictions of the model that depend on the numerical values of the eigenvalues. Before we dive into the details of these comparisons we want to convey to the reader an intuition about the meaning of the eigenvalues. One can think of a single eigenvalue as specifying the "speed" of the system (ignoring the fact that we have two eigenvalues for now). By speed we mean two things, depending on whether the dynamics is probed with perturbations or noise. (1) When we are looking at deterministic perturbations, the eigenvalue quantifies how long the system takes to return to the period-1 attractor. An example of this is plotted in Figure 3 where both eigenvalues equal 0.5 in absolute value. (2) When we are looking at noise, the eigenvalue quantifies how fast the autocorrelations go to zero as a function of the lag. For instance an

eigenvalue of 0.9 is considered slow, since for lag 1 the system has an autocorrelation 0.9 (it has an autocorrelation 1 at lag 0 by construction). At lag 2 it has an autocorrelation of $0.9^2 = 0.81$ etc. Taking a spurious correlation level of 0.1 this means that the system has an autocorrelation that is non-zero for many bounces. Consider in contrast a system with an eigenvalue of 0.1: The lag-1 autocorrelation is 0.1 which is already at the spurious level. Thus, the smaller the eigenvalue the faster the correlations decay to zero. Things stay essentially the same when we consider both eigenvalues. In that case, the autocorrelations are dominated by the largest eigenvalue since its correlations take longest to decay. Things also stay essentially the same when we consider complex eigenvalues. In that case we get oscillations between the state variables but the autocorrelation still decay to zero as the eigenvalue to the power of the lag.

In order to make model predictions about fluctuations, the model is extended by adding a stochastic component. Adding noise introduces small perturbations to the state variables that die out due to the stability properties of the map, albeit with specific relaxation behavior. This behavior is captured in the correlation functions of the state variables of the ball bouncing model. When the same correlation functions are determined for the data, model predictions can be tested. The strategy for this stochastic expansion of the deterministic ball bouncing map is to collect all influences occurring on a time scale faster than the time scale of the map into a noise term [17]. The mathematics is somewhat complex as the phase map is implicit. We introduce an intermediary state variable ϕ_{k+1}, which can be thought of as the noiseless phase of the next impact. This avoids a duplication of the noise effect due to the coupling of the equations. ϕ_{k+1} is the solution of the implicit phase map and is the state variable that couples into the velocity map. The next iterate of the phase map θ_{k+1} equals ϕ_{k+1} plus noise term. Thus, we propose the *stochastic ball bouncing map*:

$$v_{k+1} = (1+\alpha)a_r\omega_r\cos(\theta_{k+1}) - \alpha v_k + \frac{g\alpha}{\omega_r}(\phi_{k+1}-\theta_k) + q_v\xi_k, \quad (16)$$

$$0 = a_r\omega_r^2(\sin(\theta_k) - \sin(\phi_{k+1})) + v_k\omega_r(\phi_{k+1}-\theta_k) - \frac{g}{2}(\phi_{k+1}-\theta_k)^2, \quad (17)$$

$$\theta_{k+1} = \phi_{k+1} + q_\theta\xi_k. \quad (18)$$

The noise process $\xi_k \sim N(0,1)$ is normally distributed with zero mean and unit variance. The noise process is white, meaning that subsequent samples are serially independent. The extra model parameters q_v and q_θ denote the noise strengths of the velocity and phase dynamics respectively.

We compare experiment and model in terms of the correlation structure of the state variables. In order to understand how the correlation structure is reported, the so-called vector autoregressive systems of order one (VAR(1)) are briefly reviewed. For ease of notation, we denote the state of the system by $\mathbf{y}_k$:

$$\mathbf{y}_k = \begin{pmatrix} v_k - \tilde{v} \\ \theta_k - \tilde{\theta} \end{pmatrix}.$$

Note that the stationary state is subtracted, thus $\tilde{\mathbf{y}} = \mathbf{0}$, i.e., the fixed point of the state variable $\mathbf{y}_k$ is at zero. The covariance matrix $R_{yy}(l)$ as a function of lag

l is obtained as:

$$R_{yy}(l) = E[\mathbf{y}_{k+l}\mathbf{y}_k^T] = \begin{pmatrix} E[(v_{k+l} - \tilde{v})(v_k - \tilde{v})] & E[(\theta_{k+l} - \tilde{\theta})(v_k - \tilde{v})] \\ E[(v_{k+l} - \tilde{v})(\theta_k - \tilde{\theta})] & E[(\theta_{k+l} - \tilde{\theta})(\theta_k - \tilde{\theta})] \end{pmatrix}.$$

with $E[]$ denoting the expectation operator and ^{T} the matrix transpose. When the noise strengths q_v and q_θ are small, $\mathbf{y}_k$ is subject to the linearized dynamics:

$$\mathbf{y}_{k+1} = J\mathbf{y}_k + \epsilon_k, \tag{19}$$

with J the Jacobian of eq. 9. The noise vector ϵ_k has covariance matrix:

$$\begin{aligned} R_{\epsilon\epsilon}(0) &= \begin{pmatrix} q_v^2 & 0 \\ 0 & q_\theta^2 \end{pmatrix}, \\ R_{\epsilon\epsilon}(l) &= \begin{pmatrix} 0 & 0 \\ 0 & 0 \end{pmatrix} l > 1. \end{aligned}$$

The covariance matrix of the linearized system can be found from eq. 19 by multiplying both sides of the equation with $\mathbf{y}_k^T$ and taking the expectation:

$$R_{yy}(1) = E[\mathbf{y}_{k+1}\mathbf{y}_k^T] = JE[\mathbf{y}_k\mathbf{y}_k^T] = JR_{yy}(0),$$

where we used the fact that the noise has a zero-mean, i.e., $E[\epsilon_k] = 0$. It follows by iteration:

$$R_{yy}(l) = J^l R_{yy}(0).$$

The essence of this result is that the covariance function as a function of lag l behaves like the linearized dynamics as a function of iteration in that the covariance is reduced by the Jacobian J for every unit increase in the lag. Since the size of J is determined by the eigenvalue with the largest absolute value this means that the covariance is reduced by the absolute value on each lag. One minor detail in how the covariance structure is reported should be mentioned: since the units of the covariance matrix are the units of the state variables squared, it is customary to normalize them by the standard deviations. Therefore, the resulting correlation matrix has values that are necessarily between -1 and 1 and the lag-0 autocorrelations of each of the state variables equals 1.

In order to compare the model's autocorrelation functions to data, an experiment was performed in which experienced subjects performed rhythmic bouncing movements in the physical set-up of Sternad et al. [14]. Three trials of 40 s each were recorded. The coefficient of restitution was 0.42 and the acceleration of gravity was 5.8 m/s^2 (because the ball was suspended from a boom g was lower than 9.8 m/s^2). The average racket amplitude was 0.076 m and the racket period was 0.53 s. From the recorded time series of racket and ball position we extracted the ball velocity just after impact v_k and the racket phase of impact θ_k and calculated the autocorrelation functions. They are plotted in Figure 8 as grey curves. The top left panel shows the autocorrelation function of the velocity after impact, with the error bars denoting the standard deviations calculated across the three repetitions. As can be seen only the lag-0 autocorrelation of velocity after impact is different from zero. The bottom right panel shows the autocorrelation function of phase, with essentially the same finding as for the velocity after impact.

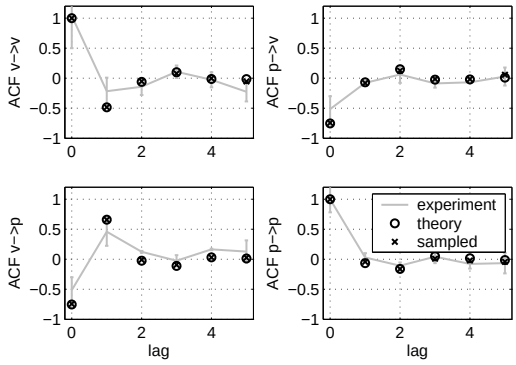

Figure 8: Observed (grey lines), theoretical (black circles) and sample (black x's) autocorrelation functions (ACF) of ball velocity after impact and racket phase of impact. Error bars denote standard deviation.

The two other panels show the crosscorrelation functions. The bottom left panel shows the correlation from velocity to phase. There is a significant negative lag-0 crosscorrelation and a significant positive lag-1 crosscorrelation. The negative lag-0 crosscorrelation can be understood as follows: imagine the phase is by chance increased relative to the stationary value ($\tilde{\theta}$), then the racket velocity will be lower (because acceleration is negative), thus imparting a lower ball velocity. Similarly, if the phase is by chance decreased, then the racket velocity is higher, imparting a higher ball velocity. In short, increased phase leads to lower velocity and vice-versa, thus the lag-0 crosscorrelation is negative. The positive lag-1 crosscorrelation can be understood similarly: if the velocity of the ball is by chance higher than the stationary value ($\tilde{v}$), then on the next cycle it will arrive later, implying an increased phase of the racket. The same logic holds for a lower velocity. The top right panel shows the correlation from phase to velocity, i.e., a fluctuation in phase leads to a later fluctuation in velocity. Only the lag-0 crosscorrelation is significantly different from zero, a fact that was already discussed above.

The correlation functions from the model were obtained in two ways: First, we sampled from the stochastic ball bouncing model (eqs. 16, 17 and 18) and calculated sample correlation functions. These sampled correlation functions are indicated in Figure 8 with crosses. Second, we calculated the autocorrelations of the linearized model (eq. 19) in closed form [11, p 21]. These linearized correlation functions are indicated in Figure 8 with circles. Note that the theoretical (circles) and sampled (crosses) autocovariance functions are so close that it is hard to discriminate the symbols. As deterministic parameters for the theoretical predictions the following values were used: $\alpha = 0.42$, $g = 5.8$ m/s^2, racket amplitude $a_r = 0.065$ m, and racket frequency $\omega_r = 2\pi/0.55$ rad/s. The value of the racket amplitude was slightly tweaked from its observe value of 0.076 m in order to get a better fit between observed and theoretical autocorrelation functions. For the stochastic parameters the following values were used: $q_v = 0.04$ m/s and $q_\theta = 0.05$ rad. These parameters were adjusted to get an agreement between observed and

theoretical standard deviations of the state variables. More precisely, we observed 0.07 m/s and 9.2 deg as standard deviations of velocity and phase resp. Theoretically, we obtained standard deviations of 0.068 m/s and 8.4 deg for velocity and phase, respectively. Returning to Figure 8, a close agreement between theory and experiment can be discerned. All predicted correlations are within one standard deviation from the experimentally observed ones. These new data underscore the previous finding that human actors exploit the stable regime. One last remark is in place: the linearized stochastic ball bouncing map (eq. 19) does an excellent job of describing the correlation functions. This can be seen from the close correspondence of the sampled correlations and the ones obtained in closed form from the linearized map. This means that the noise strengths q_v and q_θ are so low that the system stays close to the fixed point. Thus, the fluctuations during a steady state performance are so small that only linear behavior is observed. In order to force the system further away from the period-1 attractor, larger perturbations are needed, which will be the topic the next section.

7 Finer-grained predictions: relaxation behavior after perturbations

To force the system further away from the period-1 attractor, we proceed to examine the relaxation behavior of the model after introducing short perturbations to a state variable. This so-called impulse response is compared with data from an experiment with perturbations. In the experiment, experienced subjects performed rhythmic bouncing movements in the virtual set-up [4]. With the coefficient of restitution α set to 0.5, the ball was perturbed at every fifth bounce by transiently setting α to a higher or lower value than 0.5, randomly chosen from the range 0.3-0.4 or 0.6-0.7. Thus, the time of the perturbation was predictable, but the sign and the size were not. A change of α is equivalent to changing the ball velocity after impact, as will be shown below.

Figure 9 illustrates the outcome of the perturbation experiment for a single subject, shown by the black line. The data are the average values of velocity and phase for the impacts at and following the two types of perturbations. The ball velocity after impact relaxes back to the stationary value (indicated by the dashed line) after the first iteration. The phase of impact is similarly perturbed away from the stationary state in iteration 1, but relaxes back to the stationary value by iteration 2.

How does the model compare with these new data? For the theoretical analysis perturbations were applied to the initial value of the ball velocity after impact, denoted by v_0. Since the velocity was perturbed by perturbing the value of the coefficient of restitution, we need to express the perturbation of velocity in terms of the perturbed coefficient of restitution. Denoting the perturbed value of the coefficient of restitution by α_p, we find the initial velocity of the ball after impact:

$$v_0 = (1 + \alpha_p) a_r \omega_r \cos(\tilde{\theta}) - \alpha_p v_k + \frac{g\alpha_p}{\omega_r}(2\pi).$$

Substituting the stationary values of impact velocity $\tilde{v}$ and phase $\tilde{\theta}$ from eqs. 7

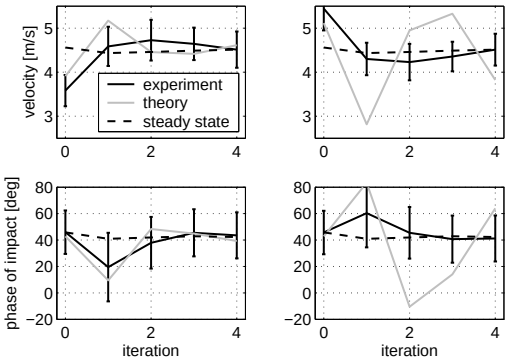

Figure 9: Average relaxation (impulse response) of phase and velocity after perturbation. The grey curves show the model, the black curves show the data for a single subject. Error bars denote the standard deviations and the dashed curves denote the stationary values of $\tilde{v} = 4.5$ m/s and $\tilde{\theta} = 42$ deg, averaged for each bounce after the perturbation. Left panels: Perturbation with a coefficient of restitution α in the range 0.3-0.4, leading to a lower velocity after impact. Right panels: Perturbation with α in the range 0.6-0.7, leading to a higher velocity after impact.

and 8, we find:

$$v_0 = \frac{1 + 2\alpha_p - \alpha_0}{1 + \alpha_0}\tilde{v},$$

with α_0 denoting the value of the coefficient of restitution for the preceding steady state behavior. Note that for this analysis we return to the deterministic model for simplicity. For the simulations of the impulse response, α_0 was set to 0.5. The values for frequency and amplitude of the racket were chosen to be identical to the ones of the corresponding experiment: $\omega_r = 2\pi/0.92$ rad/s and $a_r = 0.3$ m. The value of the acceleration of gravity was $g = 9.81$ m/s^2. The impulse responses of the model for $\alpha_p = 0.4$ and $\alpha_p = 0.6$ are shown in Figure 9 as grey curves. Iteration (impact) 0 denotes the perturbed impact, the following 4 iterations refer to the subsequent impacts. Explicitly, the ball velocity after impact is decreased when α is lower (left panels) and increased when α is increased (right panels).

Comparing these model predictions to the data, the qualitative features are similar, especially for the direction of perturbations at iterations 1 and 2 (see Figure 9). But there are also discrepancies. For $\alpha_p = 0.6$ (right panels) the model shows larger deviations than the data, whereas the deviations are relatively minor for $\alpha_p = 0.4$ (left panels). Furthermore, the model takes longer to settle to the stationary values. Where the subject recovers from the perturbation in one iteration the model takes much longer for the $\alpha_p = 0.6$ (right panels). In fact, it is not even back at the stationary value at iteration 4. We interpret these data to mean that the relaxation behavior of the model is too slow. Expressed in modeling terms, the eigenvalues of the ball bouncing map are too large. From the stability analysis we know the eigenvalues are equal to $\alpha_0 = 0.5$ in absolute value. Judging

from the observed relaxation it seems that the observed eigenvalues are less than 0.2.

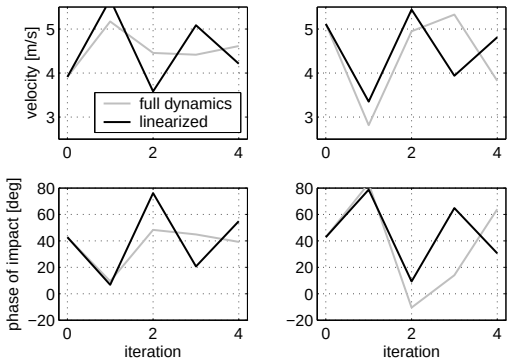

Figure 10: Comparison of the impulse response of the full ball bouncing model and the linearized model with identical Jacobians.

There are two other properties of the model that should be highlighted. The first property pertains the actual values of the perturbed coefficient of restitution α_p of 0.4 and 0.6 used in the simulation. These values of α_p are closer to the base value α_0 than the average values of α_p used in the experiment, which are 0.35 and 0.65. One can observe these smaller than average perturbations in Figure 9 in the iteration 0 values of the velocity: the theoretical curves always undershoot the experimental ones, meaning that the initial perturbation is smaller. We choose to deviate from these values since perturbations with α_p ¿ 0.65 take the system out of the domain of attraction of the period-1 attractor. In particular, $\alpha_p = 0.7$ corresponds to an initial velocity v_0 of 5.7 m/s, which is the value used in the bottom panel of Figure 3. Thus, besides being to slow, the ball bouncing model predicts a domain of attraction that is smaller than observed. This supports the notion that there are additional control mechanisms that keep the system in the stable state.

A second property pertains to the sign of the perturbation. Looking at the model relaxations in Figure 9, it seems that the relaxation takes longer in the right panels ($\alpha_p = 0.6$) as compared with the left panels ($\alpha_p = 0.4$). In a linear system there should be no difference in relaxation time for different signs of the perturbation. This difference in relaxation time is a consequence of the nonlinearity of the ball bouncing map. In Figure. 10 the relaxation of the full ball bouncing map (grey curve) is compared with its linearization (black curve) such that the Jacobians (eq. 9) of both models are identical. As one can see, the relaxation time of the linearized system is equally fast for both signs of perturbation. This shows that the asymmetry of the relaxation time of the model for the sign of the perturbation is a consequence of the nonlinearities in the dynamics. Put in modeling terms, this means that the linearized system that was used to determine linear stability is not a good approximation for perturbations of the size used in the experiment. This is in contrast to the previous section, where the linearized

system was found to give a very accurate description of the system for the noise levels observed in an experiment.

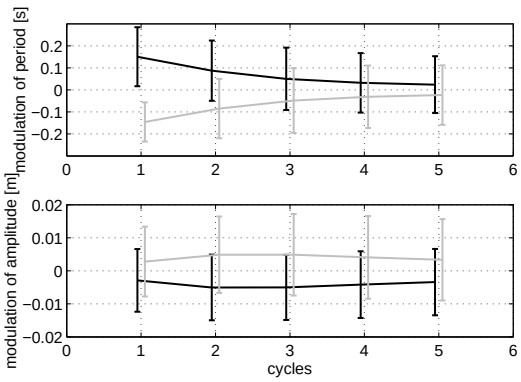

Figure 11: Modulation of racket period (top panel) and amplitude (bottom panel) in response to a perturbation of the coefficient of restitution α. The back curves indicate an increase in α, the grey curved a decrease. Each data point was calculated as the mean value of each post-perturbation impact across 10 perturbations applied within one 40 s trial. Error bars denote standard deviations.

Having identified that the ball bouncing map is too slow, the logical question is what kind of control do human actors apply to quickly equilibrate the system back to its steady state? Looking at Figure 11, we can glean further insight from additional analyses of the perturbation data. This figure shows the modulation in period and amplitude of the racket movement after a perturbation. Plotted are the differences in period and amplitude at each post-perturbation impact compared to the average period and amplitude computed over all cycles. Note that the racket period and amplitude are parameters in the model ($2\pi/\omega_r$ and a_r) and should in principle be constant. However, the data show that the racket period is increased or decreased at the first and second impact in response to the perturbation. The period modulation is such that the next impact occurs at a phase closer to the stationary value. This can be understood as follows: for an increase in α_p, the velocity with which the ball leaves the racket is higher and thus the ball flight time is longer. Therefore, the racket cycling period is increased. Hence, at the next bounce the ball hits the racket at the correct stationary phase, re-establishing the stationary state. Interestingly, the amplitude does not show similar modulations.

In a different context of modeling de Rugy et al [4] already showed that explicit period control can reproduce the basic features of these data. In the present model period control could be accommodated by making the racket frequency a third state variable. As such, frequency is no longer a fixed parameter but would obey its own dynamic state equation like the velocity after impact v_k and phase of impact θ_k. This extension, however, is left for future study.

8 Discussion

Research on human motor behavior has for a long time sought to understand coordination in terms of control mechanisms embedded within the biological system. This approach, however, has been recently augmented by the study of the dynamics of the interaction of the biological system with the environment. For instance, the simple task of freely oscillating a limb in the gravitational field revealed that subjects tend to oscillate at the resonant frequency [6]. Support for the ability to attune to dynamical properties of the actor-environment system is further supplied by its relatively early appearance in child development. Indeed, babies proved to be capable to quickly find the resonant frequency of an elastic bouncing support [5]. Not only does the resonant frequency offer the maximum response to a given level of applied torque, it also provides more stable behavior than when moving at different frequencies [5, 20].

Such stability issues become crucial for the coordination of more complex movements that involve control of many joints as in walking or running. Dynamical analysis of legged locomotion has revealed that a completely passive mechanical system can exhibit stable locomotion when solely subject to the force of gravity [10]. This phenomenon, known as passive dynamic walking, provides a good example of a stable regime that exists at the interaction of the individual with the environment. From a control point of view, such a passively stable regime has the advantage that it maintains stability with no or minimal feedback.

While this issue is intuitive, to date only few studies in motor control have pursued this hypothesis that humans take advantage of an identified stable regime and analyzed this with a formal task analysis. The present line of experiment provides an attempt to do this. More specifically, we developed a model of the ball bouncing task that is completely open-loop, i.e., with no feedback control. From this model, we derived predictions and opened the dialogue with experimental data. This dialogue confirmed that humans indeed exploit the stable regime that exists in the dynamics of the task. But it also revealed that this regime had to be, and is de facto, supported by an explicit control mechanism.

Sternad and colleagues have provided evidence for the presence of dynamical stability in a ball bouncing task [15, 13, 14, 9]. Central to their argument was the model's prediction that a passively stable regime is obtained with negative racket acceleration at impact. This prediction was confirmed in several studies using different conditions and experimental set-ups. In the present study we detailed the stability analysis, extracting new predictions, and extended it by a stochastic component. Among the new features explored with the model is the coexistence of a sticking solution together with the period-1 attractor that is established to achieve the task. While the conditions for period-1 attractor are potentially satisfied, the sticking solution may occur depending on the initial conditions. This highlights that a model that is totally free of control of the racket trajectory cannot guarantee that the period-1 attractor will be reached. This finding lead to the conclusion that a certain form of control cannot be avoided, i.e., at least during the beginning of the task when the period-1 attractor is established. It raises the important question of how passive stability is combined with control mechanism and how it adjusts with respect to perceptual information available to establish

and maintain this stability.

Exploitation of this stable regime by human actors was further confirmed in a new set of experimental data that revealed a decrease in the variability of the bouncing behavior simultaneous with a trend toward more negative values of the racket acceleration at contact. Specific to the present model is the derivation of the relation between racket amplitude and the period of the bouncing behavior. This relation was evaluated with a new set of experimental data. The stochastic version of the model permitted to derive predictions about the covariance structure of the state variables. The predicted covariance structure closely mimicked the experimentally observed one, providing more support for the ball bouncing model.

Indication for an additional control mechanism came from the relaxation behavior following a perturbation. Comparison of the model with experimental data for the velocity of the ball after impact and the phase of the impact revealed that the relaxation was slower in the model than in the experiment. This fact parallels other findings on fast relaxation after perturbations. Jindrich and Full [8] observed that walking cockroaches are able to recover from lateral perturbations and regain their heading direction faster than would be expected if neural feedback corrections were assumed. The neural reflex delay was estimated to be considerably faster than the observed corrective behavior. The authors hypothesized that this fast recovery to be caused by "preflexes", i.e. passive stabilization by means of the visco-elastic properties of the musculo-tendinous tissues. In a task where human subjects balance a pole on their finger Cabrera and Milton [3] observed control on all time scales, including corrections that were faster than the shortest feedback delays. They hypothesized this fast control to be due to parametric noise. Both of these explanations, parametric noise and passive visco-elastic properties, are possible routes for extending the ball bouncing model. We pursued a third route by examining whether the parameters of the model are constants in the experiment. We found that subjects modified the racket period in relation to the perturbation applied, while leaving the amplitude largely unchanged. This represents an important indication for a possible control of racket period or frequency. De Rugy et al. [4] proposed a neuro-mechanical model to account for this experimental feature. The period of the neural oscillator that drives a mechanical limb (forearm holding a racket) for bouncing the ball was regulated on the basis of the ball trajectory, in order to supplement the stable regime and ensure that it was maintained despite of the perturbation. This model added to the behavioral level by incorporating neurophysiological and mechanical features. But at the same time, it became more complex and difficult to analyze. In this respect, the implementation of a control mechanism within the framework developed in the present study constitutes a more economical route. One suggestion comes to mind at this point: earlier we rejected the control-theoretic approach of Bühler and Koditschek [1, 2] who suggested the mirror algorithm, where ball and racket velocity were controlled in a mirror-like fashion leading to positive racket accelerations at impact. However, the mirror algorithm does achieve stable bouncing from a wide range of inital conditions. As an extension to passive stability strategy, a period-controller based on the mirror algorithm might be a fruitful extension of the current research.

Acknowledgments This work was supported by National Science Foundation

grant SBR-9809447 awarded to Tjeerd Dijkstra and National Science Foundation grant BCS-0096543 awarded to Dagmar Sternad. Discussions with Gregor Schöner and contributions from Kunlin Wei are gratefully acknowledged.

References

[1] M. Bühler, and D.E. Koditschek, From stable to chaotic juggling: theory, simulation and experiments, In: Proc. IEEE Int. Conf. on Robotics and Automation, Cincinnati OH (1990), 1976-1981.

[2] M. Bühler, D.E. Koditschek, and P.J. Kindlmann, Planning and control of robotic juggling and catching tasks, *Int. J. Rob. Res.* 13 (1994), 101-118.

[3] J.L. Cabrera and J.G. Milton, On-off intermittency in a human balancing task, *Phys. Rev. Lett.* 89 (2002), 158702.

[4] A. de Rugy, K. Wei, H. Müller and D. Sternad, Actively tracking "passive" stability in a ball bouncing task, *Brain Res.* 982 (2003), 64-78.

[5] E.C. Goldfield, B.A. Kay and W.H. Warren, Dynamics and control of bipedal locomotion, *Child Devel.* 64 (1993), 1128-1142.

[6] N.G. Hatsopoulos and W.H. Warren, Resonance tuning in rhythmic arm movements, *J. of Motor Behav.* 28 (1996), 3-14.

[7] M.H. Hirsch and S. Smale, Differential equations, dynamical systems, and linear algebra, Academic Press, San Diego CA, 1974.

[8] D.L. Jindrich and R.J. Full, Dynamic stabilization of rapid hexapedal motion, *J. of Theor. Biology* 205 (2002), 2803-2823.

[9] H. Katsumata, V. Zatsiorsky and D. Sternad, Control of ball-racket interactions in rhythmic propulsion of elastic and non-elastic balls, *Exp. Brain Res.* 149 (2003), 17-29.

[10] T. McGeer, Dynamics and control of bipedal locomotion, *J. of Theor. Biol.* 163 (1993), 277-314.

[11] H. Lütkepohl, Introduction to multiple time series analysis, 2d ed, Springer-Verlag, Berlin, 1993.

[12] W.H. Press, B.P. Flannery, S.A. Teukolsky and W.T. Vetterling, Numerical Recipes in C, Cambridge University Press, Cambridge UK, 1988.

[13] D. Sternad, M. Duarte, H. Katsumata and S. Schaal, Dynamics of bouncing a ball in human performance, *Phys. Rev. E* 63 (2000), 011902.

[14] D. Sternad, M. Duarte, H. Katsumata and S. Schaal, Bouncing a ball: tuning into dynamic stability, *J. of Exp. Psych.: Hum. Perc. and Perf.* 27 (2001), 1163-1184.

[15] S. Schaal, C.G. Atkeson and D. Sternad, One-handed juggling: a dynamical approach to a rhythmic movement task, *J. of Motor Behav.* 28 (1996), 165-183.

[16] E.R. Scheinerman, Invitation to dynamical systems, Prentice-Hall, Upper Saddle River NJ, 1996.

[17] G. Schöner, H. Haken and J.A.S. Kelso, A stochastic theory of phase transitions in human hand movement, *Biol. Cybern.* 53 (1986), 247-257.

[18] S.H. Strogatz, Nonlinear dynamics and chaos, Addison-Wesley, Reading MA, 1994.

[19] N.B. Tufillaro, T. Abbott and J. Reilly, An experimental approach to nonlinear dynamics and chaos, Addison-Wesley, Redwood City CA, 1992.

[20] H. Yu, D.M. Russell and D. Sternad, Task-effector asymmetries in a rhythmic continuation task, *J. of Exp. Psych.: Hum. Perc. and Perf.* 29 (2003), 616-630.